HHS Public Access

Author manuscript

Cell Rep Phys Sci. Author manuscript; available in PMC 2023 July 26.

Published in final edited form as:

Cell Rep Phys Sci. 2022 December 21; 3(12): . doi:10.1016/j.xcrp.2022.101185.

Rapid hydrogel formation via tandem visible light photouncaging and bioorthogonal ligation

Kun-You Chung[1], **Kathleen N. Halwachs**[2], **Pengtao Lu**[1], **Kaihong Sun**[1], **Hope A. Silva**[1], **Adrianne M. Rosales**[2], **Zachariah A. Page**[1,3,*]

[1]Department of Chemistry, The University of Texas at Austin; Austin, TX 78712, USA

[2]McKetta Department of Chemical Engineering, The University of Texas at Austin; Austin, TX 78712, USA

[3]Lead contact

SUMMARY

The formation of benign polymer scaffolds in water using green-light-reactive photocages is described. These efforts pave an avenue toward the fabrication of synthetic scaffolds that can facilitate the study of cellular events for disease diagnosis and treatment. First, a series of boron dipyrromethene (BODIPY) photocages with nitrogen-containing nucleophiles were examined to determine structure-reactivity relationships, which resulted in a >1,000× increase in uncaging yield. Subsequently, photoinduced hydrogel formation in 90 wt % water was accomplished via biorthogonal carbonyl condensation using hydrophilic polymer scaffolds separately containing BODIPY photocages and ortho-phthalaldehyde (OPA) moieties. Spatiotemporal control is demonstrated with light on/off experiments to modulate gel stiffness and masking to provide <100 μm features. Biocompatability of the method was shown through pre-/post-crosslinking cell viability studies. Short term, these studies are anticipated to guide translation to emergent additive manufacturing technology, which, longer term, will enable the development of 3D cell cultures for tissue engineering applications.

Graphical Abstract

*Correspondence: zpage@utexas.edu.

AUTHOR CONTRIBUTIONS

Conceptualization, K.-Y.C. and Z.A.P.; methodology, K.-Y.C., P.L., K.S., H.A.S., K.N.H., A.M.R., and Z.A.P.; investigation, K.-Y.C., P.L., K.S., H.A.S., and K.N.H.; visualization, K.-Y.C., K.N.H., and Z.A.P.; funding acquisition, A.M.R. and Z.A.P.; project administration, Z.A.P.; supervision, A.M.R. and Z.A.P.; writing – original draft, K.-Y.C., A.M.R., and Z.A.P.; writing – review & editing, K.-Y.C., P.L., K.S., H.A.S., K.N.H., A.M.R., and Z.A.P.

SUPPLEMENTAL INFORMATION

Supplemental information can be found online at https://doi.org/10.1016/j.xcrp.2022.101185.

DECLARATION OF INTERESTS

The authors declare no competing interests.

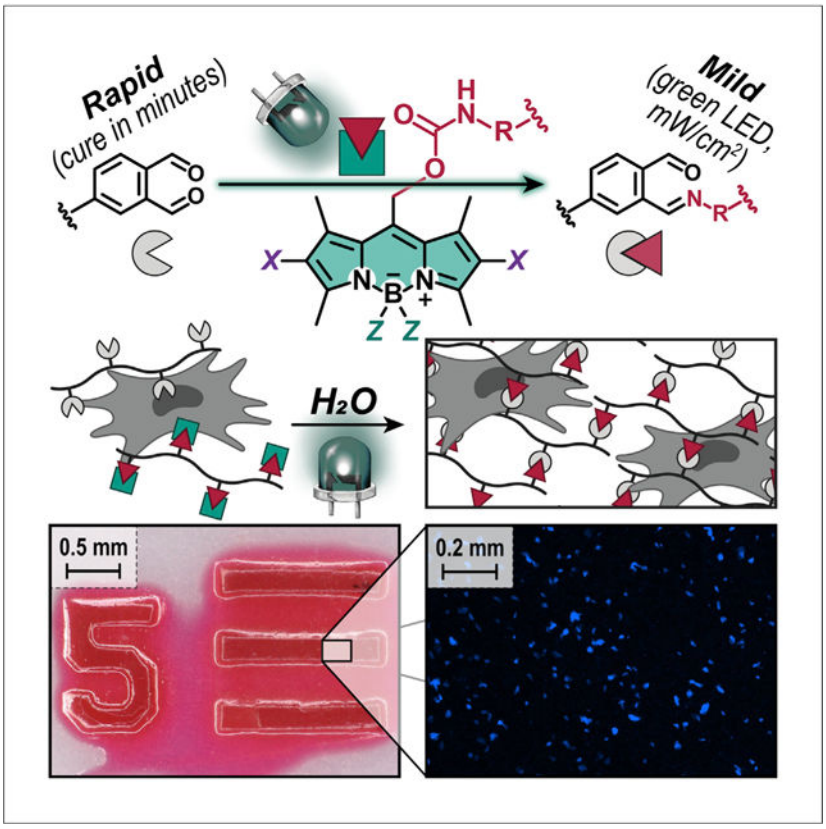

Chung et al. describe efficient and mild chemistry to create water-swollen polymer networks using green LEDs. These findings may inform the development of advanced tissue culture technology to study cellular events for improved disease diagnosis and treatment.

INTRODUCTION

Light is an ideal stimulus for the preparation of materials with well-defined geometric structures, such as patterned 2D films and 3D objects.[1] This arises from the inherent spatiotemporal control offered by light-driven (photochemical) reactions or the ability to define when and where a chemical transformation takes place. Photouncaging, light-induced unveiling of protected functional groups to release target molecules (cargo),[2–5] represents one such photochemical transformation. Relative to commonly employed homolytic photolysis to generate highly reactive carbon-centered radicals,[6–8] photouncaging offers potentially milder and more benign conditions to facilitate biological implementation. To this end, photouncaging has been used to examine short-lived cellular events,[9] control drug release,[10] and fabricate biomaterials, such as water-swollen polymer networks (hydrogels), for tissue engineering.[11,12] However, these examples traditionally rely on the use of short wavelength (<400 nm) UV light for activation, which mitigates widespread utility in biomedical applications. This hurdle arises from shallow UV light penetration in biomaterials due to abundant absorption/scattering events and concomitant cytotoxicity.[13–15] As such, research efforts have recently shifted toward a spectral expansion of photouncaging to encompass longer wavelength visible light (~400–700 nm).

Visible light photouncaging represents an attractive alternative to UV light due to reduced biomaterial interactions and therefore holds promise to increase photon penetration depth and reduce cytotoxicity.[9,16] Moreover, absorption specificity of chromophores is greatly pronounced in the visible spectral region relative to UV, where chromophore absorption is nearly ubiquitous. This facet, coupled with the recent industrialization of efficient, inexpensive, and narrow-band visible LEDs, paves an avenue toward wavelength-selective reactivity where final material properties are dictated by the color of incident light exposure.[17–25] Such wavelength-selective chemistry promises to enable, for example, the fabrication of multifunctional soft materials with a myriad of applications ranging from tissue engineering to soft robotics. Despite these advantages, few reports exist on biocompatible materials fabrication via uncaging and subsequent ligation with visible light.[12] Moreover, the lack of a systematic study correlating structure to photoligation efficiency presents an opportunity to identify governing design principles that can inform more rapid preparation of biomaterials for additive manufacturing, where speed is paramount to lower production costs, maximize resolution,[26] minimize deleterious light-matter interactions, and create homogeneous cell-laden biomimetic scaffolds.

As a foundation for visible light photouncaging, boron dipyrromethene (BODIPY) derivatives have recently emerged as promising candidates.[27–29] This arises from the structural rigidity and synthetic modularity of BODIPYs, which provide optoelectronic tunability for strong absorption across a wide wavelength range (~500–900 nm) and efficient heterolytic photolysis at the meso-methyl bridgehead position.[30] To this end, Winter and coworkers have carefully examined photocages and identified structural motifs that greatly improve uncaging efficiency, primarily with respect to halide, acetate, and alcohol cargo (Figure 1A).[31–35] Key findings to increase uncaging efficiency include (1) boron methylation for inductive stabilization of the meso-methyl carbocation; (2) pyrrole halogenation for enhanced intersystem crossing (ISC) rates (heavy atom effect)[36] to long-lived triplet excited states (e.g., I > Br > Cl); (3) selecting stable leaving groups (e.g., Cl^- > AcO^- > MeO^-); and (4) ring fusion for decreased internal conversion and concomitant excited-state relaxation. These findings inspired the present examination of BODIPY photocages for the release of nucleophilic amino functionality and their utility in rapid bioorthogonal conjugation chemistry to form hydrogels.

Biocompatible synthetic hydrogels have been predominantly prepared from chain-end functionalized 4-arm star poly(ethylene oxide) (PEO) derivatives.[37] However, the polymer precursors are challenging to synthesize and thus difficult to scale. Side-chain functionalized hydrophilic poly(meth)acrylates represent an attractive alternative platform with potential scalability via (controlled) radical polymerization from inexpensive hydrophilic monomers. Specifically, compared with anionic polymerization used to synthesize PEO, (controlled) radical polymerization provides greater functional group tolerance and modularity (i.e., comonomer feedstock ratio as opposed to the number of chain ends).

Irrespective of the specific polymer composition and architecture, thematic ligation strategies to form hydrogels have emerged in the literature.[38–40] These include the formation of oximes from aminooxy/aldehyde,[38,41–45] sulfides from thia-Michael,[7,8,46] and heterocycles from strain-promoted addition (e.g., azide-alkyne and tetrazine-

norbornene).[13,40,47–49] In these systems, the time to gelation directly correlates with the rate constants for each reaction, which differ as much as ~5 orders of magnitude. Specifically, rates vary from 10^{-2} $M^{-1}s^{-1}$ for aminooxy/aldheyde to ~10^2–10^3 $M^{-1}s^{-1}$ for the tetrazine ligation.[47,49] As precedent, Truong and coworkers recently reported the preparation of hydrogels by photoinduced thia-Michael addition (Figure 1B).[12] In this report, 4-arm star PEOs were independently functionalized with BODIPY photocages and propiolate, which were coupled upon irradiation with green light.[12] More recently, Truong, Barner-Kowollik, and coworkers demonstrated coupling of chain-end functionalized 4-arm star PEOs using red-light-driven aminooxy/aldehyde hydrogel formation, where the aldehyde functionality was revealed via photooxidation of furan.[50] Additionally, Chen, He, and coworkers demonstrated non-photochemical ortho-phthalaldehyde (OPA) condensation as a strategy to rapidly form hydrogels,[45] again using chain-end functionalized 4-arm star PEOs. This built upon the discovery by Gillingham and coworkers in 2014 where aminooxy/OPA ligation was found to have a rate constant of 10^2 $M^{-1}s^{-1}$, which is ~4 orders of magnitude faster than aminooxy/aldehyde coupling.[49]

The present report describes the synthesis and quantitative characterization of BODIPY photocages comprising amine, hydrazine, and aminooxy cargo, along with their utility in rapid and mild hydrogel formation via OPA condensation from side-chain functionalized hydrophilic polymers (Figure 1C). The reaction quantum yields for one-pot photouncaging and OPA ligation with 6 different BODIPY photocage derivatives exposed to green LEDs (~520 nm) is reported, and cytocompatibility of the photouncaging and ligation process is demonstrated. These findings provide structure-reactivity relationships that will inform the design of next-generation photocages for use in soft materials fabrication and/or functionalization.

RESULTS

Photocage design and synthesis

The initial design parameters surrounded the use of BODIPY as a modular photoprotecting group for nucleophilic cargo capable of rapid and biocompatible ligation upon uncaging. Specifically, BODIPY derivatives were synthesized considering three motifs (Scheme 1): (1) leaving group (*LG*) basicity/nucleophilicity, (2) pyrrole halogenation, and (3) boron methylation. Following literature precedent,[10,35,51] meso-methylacetyl BODIPY (**1**) was synthesized via the condensation of 2,4-dimethyl-1*H*-pyrrole and 2-chloro-2-oxoethyl acetate with $BF_3{\cdot}OEt_2$. Hydrolysis of the acetyl group with NaOH or MeMgBr provided compound **2**, where *Z* = F or Me, respectively. Reaction of the alcohol on compound **2** with 4-nitrophenyl chloroformate yielded compound **3**, followed by bromination with *N*-bromosuccinimide to provide derivatives where *X* = Br. Finally, substitution with benzyl-amine (*Am*), -hydrazine (*Hy*), or -aminooxy (*Ox*) provided the desired BODIPY photocages.

For the *LG* design, carbamate linkages at the meso-methyl (bridgehead) position were installed to facilitate photolysis, followed by rapid decarboxylation to unveil the nucleophilic nitrogen containing small molecules (Scheme 1). As a second design parameter, pyrrole halogenation (*X* = H versus Br) was selected to facilitate ISC from short-lived spin-singlet (ñanosecond) to long-lived spin-triplet (~microsecond) excited states to increase the

likelihood of photolysis for each photon absorbed. Additionally, boron methylation (*Z* = Me versus F) was selected as a third design parameter to decrease the activation energy barrier to photolysis by inductively stabilizing the meso-methyl carbocation intermediate. The influence of these design parameters on photophysical properties and photouncaging quantum yields were subsequently characterized to inform the selection of BODIPY photocages for materials fabrication.

Photocage photophysics

Steady-state photophysical properties for each photocage were characterized as an initial step toward quantifying uncaging quantum yield. As shown in Figure 2A, UV-visible absorption spectroscopy revealed a signature BODIPY absorption band for all photocages in the green light spectral region (~500–550 nm). All derivatives were strongly absorbing with extinction coefficients measured between 50,000 and 70,000 M^{-1} cm^{-1} (Table S1). Notably, exchanging fluorine for methyl groups on the boron (*Z* = F to Me) resulted in a blue-shifted peak absorption (~10 nm), while halogenation (*X* = H to Br) resulted in a red shift (~23 nm). In contrast, the *LG* did not significantly influence absorption profiles (Figure S45; Table S1). Underlaying the green LED emission profile with the BODIPY absorption profiles highlights the variance in photons absorbed (γ_A) by different derivatives. Quantifying γ_A for the BODIPY-*ZX*-*Am* series provided -*FBr*- R -*MeBr*- > -*FH*- ≈ -*MeH*-, with normalized values of 1, 0.99, 0.77, and 0.77, respectively (Figure 2A, inset). These values were used to calculate photouncaging quantum yields (described later).

Photoluminescence spectroscopy was used to quantify the fluorescence quantum yield (Φ_f) for each derivative to gain insight into competitive non-radiative relaxation pathways, such as those that would arise from ISC to spin-triplet excited states (Figure 2B). Both methylation (*Z* = Me) and halogenation (*X* = Br) resulted in dramatic decreases in Φ_f. Specifically, the trend for the BODIPY-*ZX*-*Am* series was -*FH*- (Φ_f ~ 1) > -*MeH*- (Φ_f = 0.25) > -*FBr*- (Φ_f = 0.19) > -*MeBr*- (Φ_f = 0.05) (Figure 2B, inset). Notably, exchanging -*Am* with -*Hy* or -*Ox* functionality did not significantly alter Φ_f (Figure S45; Table S1). At this stage, it was hypothesized that the decrease in Φ_f upon methylation and halogenation would correlate with increased triplet yields to facilitate photouncaging.

Photouncaging efficiency

To determine photouncaging quantum yields, steady-state photolysis experiments were undertaken. Each BODIPY photocage was placed in dilute solution (0.53 mM in 4:1 CH_3CN:H_2O), degassed with argon, and irradiated with a green LED (λ_{max} = 520 nm, ~10 mW/cm^2). Aliquots were removed at 1, 2, 4, 7, and 12 min intervals, and the disappearance of each BODIPY photocage was assessed using high-performance liquid chromatography (HPLC), followed by quantification using a photodiode array detector and the previously determined extinction coefficients for each BODIPY photocage derivative. As shown in Figure 3A, the rate of BODIPY-*ZX*-*Am* consumption increased in going from -*FH*- < -*FBr*- < -*MeH*- < -*MeBr*-. Under the present conditions, little to no photodegradation was observed for the -*FH*- derivative after 12 min of irradiation (~3% after 1 h; see Figure S46 and Table S1). In contrast, quantitative consumption was observed in just over 12 min for the -*MeH*- derivative (Figure S48) and just under 7 min for the -*MeBr*-derivative (Figure

S49). These results provided indirect evidence that both pyrrole bromination and boron methylation may increase photouncaging quantum yield, with the latter (methylation) being more influential. Following the same protocol, the rate of consumption for the BODIPY-*MeBr*-*LG* series revealed a moderate increase in rate going from -*Am* < -*Hy* < -*Ox* (Figure 3B). This trend is hypothesized to result from a decrease in acidity for the conjugate acids of each benzyl derivative: experimental/theoretical *pKa* ≈ 9.3[52] < 8.5[53] < 4.7,[54] respectively. Notably, BODIPY-*MeBr*-*Ox* was fully consumed within 4 min of low-intensity green light irradiation. However, this trend may arise in part or in full from increased nucleophilicity of -*Ox* and -*Hy* relative to -*Am* leading to a more pronounced substitution reaction with BODIPY chromophores post-uncaging.

To deconvolute the relationship between photobleaching and -uncaging, the products of irradiation were characterized post-HPLC separation (Figure 4). Initially, absorption calibration curves for BODIPY-CH_2OH (i.e., meso-methyl alcohol) and benzyl-*Am*, -*Hy*, and -*Ox* were created to quantify photouncaging byproducts (Figures S51–S53; Table S1). However, it was determined that poor photostability of BODIPY-CH_2OH and *N*-oxidation of the benzyl cargo post-uncaging precluded accurate quantification by this method. As an alternative approach, 1 equiv OPA relative to each BODIPY photocage was added to the solution to trap the benzyl-nucleophiles *in situ*. The stable OPA-imine, -hydrazone, and -oxime products were independently synthesized to create absorption calibration curves (along with OPA by itself) that were then used to estimate photouncaging quantum yields (Figures S55–S57; Table S1). Barring any side reactions, the rate of BODIPY photocage disappearance would match that of OPA, as well as the appearance of the OPA conjugate. As a representative case, BODIPY-*MeBr*-*Am* was irradiated in the presence of OPA, and HPLC was used to track photocage and OPA disappearance and OPA-*Am* appearance (Figure 4A). The [BODIPY-*MeBr*-*Am*] was found to decrease slightly faster than that of [OPA], while the appearance of [OPA-*Am*] tracked well with the [OPA] consumption. These results indicate that the OPA/benzylamine reaction is approximately quantitative and not rate limiting, while photouncaging is not quantitative (i.e., a portion of the photocage degrades during irradiation without releasing benzylamine) (Figure S51). Specifically, after 12 min of irradiation, >99% of the initial BODIPY-*MeBr*-*Am* and 77% ± 7% of the initial OPA had disappeared, while 72% ± 2% of OPA-*Am* had appeared. Thus, a reaction yield of ~75% is possible under the present conditions. To determine the intrinsic reaction quantum yields (Φ_{rxn}), the amount of OPA conjugate was quantified at short times (~30 s aliquots) to reveal the following: -*FH*- (Φ_{rxn} = 0.0001) < -*FBr*- (Φ_{rxn} = 0.003) < -*MeH*- (Φ_{rxn} = 0.042) < -*MeBr*- (Φ_{rxn} = 0.13) (Figure 4B). Furthermore, in altering the *LG* for BODIPY-*MeBr* photocages, the uncaging yields remained in the same order of magnitude: -*Am* (Φ_{rxn} = 0.13) < -*Hy* (Φ_{rxn} = 0.23) < -*Ox* (Φ_{rxn} = 0.39) (Table S1). Therefore, photouncaging quantum yield was increased by more than 1,000× in going from -*FH*- to -*MeBr*- functionality. As solvent polarity is increased, the excited-state intramolecular charge-transfer character would likely be enhanced, which would lead to faster decay to the ground state and, in turn, reduced photouncaging yields. However, the uncaging yields could not be measured in pure water due to solubility constraints of the small-molecule BODIPY photocages.

Hydrogel preparation and characterization

Functional copolymers were synthesized to serve as hydrogel precursors, incorporating BODIPY-*ZX*-*Am* and OPA as pendent groups within a hydrophilic poly(ethylene glycol methacrylate) (PEGMA) scaffold (Scheme 2). Specifically, a protected OPA-methacrylate (^{p}OPAMA) was synthesized from a carboxylic acid functionalized ^{p}OPA by first converting the carboxylic acid on ^{p}OPA to an activated *N*-hydroxysuccinimidyl ester,[45] reacting the active ester with ethanolamine, and then the resultant hydroxyl functionality with methacryloyl chloride. The ^{p}O-PAMA monomer was then copolymerized with PEGMA (M_n = 500 g/mol) via a free-radical method. Deprotection of the resultant copolymer with trifluoroacetic acid in water provided the desired poly(OPAMA-*co*-PEGMA). Installment of BODIPY-*ZX*-*Am* functionality was accomplished using an analogous free-radical copolymerization method between PEGMA and an Fmoc-protected β-alanine methacrylate (^{p}β-AlaMa), which was obtained via esterification of 2-hydorxyethylmethacrylate with Fmoc-β-alanine, followed by Fmoc deprotection with piperidine and reaction of the resultant primary *Am* with the para-nitrophenyl carbonate-BODIPY precursor (compound **3**; Schemes 1 and S5). Monitoring the free-radical copolymerizations with 1H-nuclear magnetic resonance (NMR) revealed similar rates of incorporation for the functional monomers relative to PEGMA, indicating the formation of statistical polymer architectures. Thus, target feed ratios of each functional monomer matched the final comonomer incorporation, which was varied to provide 6, 10, and 20 mol % relative to PEGMA. Gel-permeation chromatography (GPC) of the resultant copolymers provided number average molecular weights of ~45,000 g/mol relative to poly(methyl methacrylate) standards. All copolymers were fully water soluble and stable in aqueous solution when stored in the dark.

Mild and rapid visible-light-induced hydrogel formation was first demonstrated through a qualitative vial inversion test (Figure 5A). A mixture of poly(OPAMA-*co*-PEGMA) (5 wt %) and poly(BrBODIPYMA-*co*-PEGMA) (5 wt %) in water was placed in a glass vial and irradiated with a 520 nm LED until gelation occurred (approximately minutes). All reactive comonomer ratios (6, 10, and 20 mol %) resulted in gelation; however, 10 mol % was selected for future experimentation as it provided the best qualitative compromise between mechanical properties and time to gelation; 6 mol % provided non-self-supporting gels, and 20 mol % took longer to gel, likely due to strong attenuation of green light at such high loadings. For the 10 mol % copolymers, photorheological studies were employed to quantitatively characterize crosslinking kinetics and mechanical properties as a function of light intensity (Figure 5B). Aqueous solutions containing 5 wt % of each functionalized copolymer (i.e., 90 wt % water) were prepared and placed onto the rheometer containing a transparent bottom plate and parallel top plate. Samples were surrounded with a thin layer of oil to prevent water evaporation during measurement. Each run was performed under ambient conditions and contained an initial 15 s dark period where no significant change in storage or loss moduli (G′ and G″, respectively) was observed. Each sample was characterized in triplicate using 30, 60, 90, or 180 mW/cm^2 525 nm light intensity. Irradiation led to an increase in G' and G'', substantiating a good temporal response. The crossover of G' and G'' was taken as the gel point, which was inversely related to light intensity. Specifically, gel times (τ_{gel}) of 20 ± 7, 75 ± 18, 179 ± 16, and 217 ± 42 s were obtained for 180, 90, 60, and 30 mW/cm^2 irradiation intensities, respectively. Notably, the

final G' for the present gels was low, ~200 Pa in the linear viscoelastic region (Figure S62), which is in line with a recent report on hydrogels prepared from brush polymers[55] but may also signify a low crosslink density that could arise from steric interactions inherent to the brush architecture and the relatively short tether to the photocage. The gels appeared to be stable in PBS for several weeks, as no degradation or change in mechanical properties was qualitatively observable. Higher modulus materials could be achieved with future iterations that increase the accessibility of the photocage. Overall, short irradiation times were required to provide a self-supporting gel, with a time to G′ of 100 Pa (τ_G≈100 Pa) between 15 and 18 min depending on the light intensity used (Figure 5B).

Irradiation cycling (i.e., LED on/off) and photopatterning experiments were performed to characterize the degree of temporal and spatial control over the light-induced hydrogel fabrication approach. Temporal control was demonstrated using photorheology by cycling the green LED on and off post-gelation while monitoring G' and G'' (Figure 6A). Using a light intensity of 40 mW/cm^2, 4 × 30 s on/off irradiation cycles were carried out. Within seconds of turning the LED on, G′ increased, followed by turning the light off, resulting in immediate halting of G'. Each cycle resulted in a 2 Pa increase, demonstrating the ability to fine-tune gel stiffness (G') with the present approach, with potential utility in modulating cell-surface interactions.[56,57] This process was reproducible, and moduli could be tailored by changing light intensity. For example, 30 s on/off cycling at 160 mW/cm^2 resulted in larger steps in G' (~7 Pa) (Figure S63). Next, spatial control was tested using a negative 1951 USAF resolution test target (photomask) (Figures S64–S68). Specifically, the photopolymer solution (90 wt % water) was placed on a transparent perfluorinated sheet on glass with 250 μm plastic shims flanking the resin. The USAF photomask was placed on top of the resin, and the sample was irradiated with the green LED at 30 mW/cm^2 for 45 min. After carefully removing the photomask, excess resin was rinsed away with water, followed by acetone, and imaged with a digital microscope (Figure 6B). Well-defined, %100 μm features were observed (Figure 6Bii), with a smallest demonstrated resolution of 32 lp/mm (i.e., 16 μm discernable lines; Figure S65). The high degree of spatiotemporal control holds promise to enable 3D fabrication of microvascularized hydrogel networks for tissue engineering applications.

Cell encapsulation

The bioorthogonality of the present photoligation strategy was examined by characterizing cell viability and cell encapsulation in the hydrogel. Human mesenchymal stem cells (hMSCs) were selected for cell studies due to their relevance for cell therapies and regenerative medicine.[56] To assess cytocompatibility of the hydrogel precursors, an MTT assay was performed for cells plated with varying concentrations of poly(OPAMA-*co*-PEGMA).[57] The MTT assay revealed that poly(OPAMA-*co*-PEGMA) concentrations below 5 wt % were not significantly cytotoxic (Figure S69). To encapsulate hMSCs, hydrogels were fabricated with 5 wt % poly(OPAMA-*co*-PEGMA), 5 wt % poly(BrBODIPYMA-*co*-PEGMA), and a cell adhesive peptide, RGD[58] (2 mM), in PBS, followed by irradiating for 5 min with the green LED (600 mW/cm^2 for rapid curing) (Figure 7A). Staining with a live-cell stain (calcein blue AM) indicated that hMSCs survived the encapsulation with qualitatively high viability (Figure 7B). Attempts to image dead cells were not successful

due to background fluorescence from residual BODIPY that emits across green to red channels (500–700 nm). Staining the cells with a general fluorescent dye (Cell Tracker Blue) and imaging via confocal microscopy showed that they were distributed throughout multiple planes in the hydrogel (Figure 7C). The promising results obtained during these cell studies support the future investigation and optimization of this biorthogonal photoligation strategy for application in the field of biomaterials.

EXPERIMENTAL PROCEDURES

Resource availability

Lead contact—Further information and requests for resources should be directed to and will be fulfilled by the lead contact, Zachariah A. Page (zpage@utexas.edu).

Materials availability—All materials generated in this study are available from the lead contact without restriction.

Data and code availability—The datasets generated during this study are available in the supplemental information.

Supplementary Material

Refer to Web version on PubMed Central for supplementary material.

ACKNOWLEDGMENTS

The authors acknowledge primary support by the National Science Foundation under grant no. MSN-2107877 (K.-Y.C. and Z.A.P.). Partial support was provided by the Robert A. Welch Foundation under grant no. F-2007 (P.L., K.S., H.A.S., and Z.A.P.) and by the National Institutes of Health under grant no. R35GM138193 (K.N.H. and A.M.R.). Figure 7A contains icons generated by BioRender.com.

REFERENCES

1. Jung K, Corrigan N, Ciftci M, Xu J, Seo SE, Hawker CJ, and Boyer C (2020). Designing with light: advanced 2D, 3D, and 4D materials. Adv. Mater 32, e1903850. 10.1002/adma.201903850. [PubMed: 31788850]
2. Suyama K, and Shirai M (2009). Photobase generators: recent progress and application trend in polymer systems. Prog. Polym. Sci 34, 194–209. 10.1016/j.progpolymsci.2008.08.005.
3. Liu X, Li Z, Hu P, Dong X, Liu R, and Zhu G (2015). Thioxanthone acetic acid ammonium salts: highly efficient photobase generators based on photodecarboxylation. RSC Adv. 5, 53342–53348. 10.1039/c5ra09314g.
4. Zhang X, Xi W, Wang C, Podgórski M, and Bowman CN (2016). Visible-light-initiated thiol-Michael addition polymerizations with Coumarin-based photobase generators: another photoclick reaction strategy. ACS Macro Lett. 5, 229–233. 10.1021/acsmacrolett.5b00923. [PubMed: 28018752]
5. Weinstain R, Slanina T, Kand D, and Klán P (2020). Visible-to-nir-light activated release: from small molecules to nanomaterials. Chem. Rev 120, 13135–13272. 10.1021/acs.chemrev.0c00663. [PubMed: 33125209]
6. Echalier C, Valot L, Martinez J, Mehdi A, and Subra G (2019). Chemical cross-linking methods for cell encapsulation in hydrogels. Mater. Today Commun. 20, 100536. 10.1016/j.mtcomm.2019.05.012.

7. Shih H, and Lin CC (2012). Cross-linking and degradation of step-growth hydrogels formed by thiol-ene photoclick chemistry. Biomacromolecules 13, 2003–2012. 10.1021/bm300752j. [PubMed: 22708824]
8. Roberts JJ, and Bryant SJ (2013). Comparison of photopolymerizable thiol-ene PEG and acrylate-based PEG hydrogels for cartilage development. Biomaterials 34, 9969–9979. 10.1016/j.biomaterials.2013.09.020. [PubMed: 24060418]
9. Toupin NP, Arora K, Shrestha P, Peterson JA, Fischer LJ, Rajagurubandara E, Podgorski I, Winter AH, and Kodanko JJ (2019). BODIPY-caged photoactivated inhibitors of Cathepsin B flip the light switch on cancer cell apoptosis. ACS Chem. Biol 14, 2833–2840. 10.1021/acschembio.9b00711. [PubMed: 31750642]
10. Sitkowska K, Hoes MF, Lerch M, Lameijer L, van der Meer P, Szymanski W, and Feringa BL (2020). Red – light – sensitive BODIPY photoprotecting groups for amines and their biological application in controlling heart rhythm. Chem. Commun 56, 5480–5483. 10.1039/d0cc02178d.
11. Grim JC, Marozas IA, and Anseth KS (2015). Thiol-ene and photo-cleavage chemistry for controlled presentation of biomolecules in hydrogels. J. Contr. Release 219, 95–106. 10.1016/j.jconrel.2015.08.040.
12. Li M, Dove AP, and Truong VX (2020). Additive-free green light-induced ligation using BODIPY triggers. Angew. Chem. Int. Ed 59, 2284–2288. 10.1002/anie.201912555.
13. Nani RR, Gorka AP, Nagaya T, Yamamoto T, Ivanic J, Kobayashi H, and Schnermann MJ (2017). In vivo activation of duocarmycin-antibody conjugates by near-infrared light. ACS Cent. Sci 3, 329–337. 10.1021/acscentsci.7b00026. [PubMed: 28470051]
14. Vorobev AY, and Moskalensky AE (2020). Long-wavelength photoremovable protecting groups: on the way to in vivo application. Comput. Struct. Biotechnol. J 18, 27–34. 10.1016/j.csbj.2019.11.007. [PubMed: 31890141]
15. Silva JM, Silva E, and Reis RL (2019). Light-triggered release of photocaged therapeutics - where are we now? J. Contr. Release 298, 154–176. 10.1016/j.jconrel.2019.02.006.
16. Kand D, Liu P, Navarro MX, Fischer LJ, Rousso-noori L, Friedmann-morvinski D, et al. (2020). Water-Soluble BODIPY Photocages with Tunable Cellular Localization (J. Am. Chem. Soc) 10.1021/jacs.9b13219.
17. Corrigan N, and Boyer C (2019). 100th anniversary of macromolecular science viewpoint: photochemical reaction orthogonality in modern macromolecular science. ACS Macro Lett. 8, 812–818. 10.1021/acsmacrolett.9b00292. [PubMed: 35619516]
18. Corrigan N, Ciftci M, Jung K, and Boyer C (2021). Mediating reaction orthogonality in polymer and materials science. Angew. Chem. Int. Ed 60, 1748–1781. 10.1002/anie.201912001.
19. Bialas S, Michalek L, Marschner DE, Krappitz T, Wegener M, Blinco J, Blasco E, Frisch H, and Barner-Kowollik C (2019). Access to disparate soft matter materials by curing with two colors of light. Adv. Mater 31, 1807288. 10.1002/adma.201807288.
20. Lu P, Ahn D, Yunis R, Delafresnaye L, Corrigan N, Boyer C, Barner-Kowollik C, and Page ZA (2021). Wavelength-selective light-matter interactions in polymer science. Matter 4, 2172–2229. 10.1016/j.matt.2021.03.021.
21. Kalayci K, Frisch H, Barner-Kowollik C, and Truong VX (2020). Wavelength-dependent stiffening of hydrogel matrices via redshifted [2+2] photocycloadditions. Adv. Funct. Mater 30, 1908171. 10.1002/adfm.201908171.
22. Pelloth JL, Tran PA, Walther A, Goldmann AS, Frisch H, Truong VX, and Barner-Kowollik C (2021). Wavelength-selective softening of hydrogel networks. Adv. Mater 33, e2102184. 10.1002/adma.202102184. [PubMed: 34365684]
23. Truong VX, Bachmann J, Unterreiner AN, Blinco JP, and Barner-Kowollik C (2022). Wavelength-orthogonal stiffening of hydrogel networks with visible light. Angew. Chem. Int. Ed 61, e202113076. 10.1002/anie.202113076.
24. Rapp TL, and DeForest CA (2020). Visible light-responsive dynamic biomaterials: going deeper and triggering more. Adv. Healthc. Mater 9, 1–15. 10.1002/adhm.201901553.
25. Rapp TDC (2022). Tricolor visible wavelength-selective photodegradable hydrogel biomaterials. Preprint at ChemRxiv. 10.26434/chemrxiv-2022-hlbk6.

26. Bagheri A, and Jin J (2019). Photopolymerization in 3D printing. ACS Appl. Polym. Mater 1, 593–611. 10.1021/acsapm.8b00165.
27. Zhang XF, and Yang X (2013). Photosensitizer that selectively generates singlet oxygen in nonpolar environments: photophysical mechanism and efficiency for a covalent BODIPY dimer. J. Phys. Chem. B 117, 9050–9055. 10.1021/jp405102m. [PubMed: 23837434]
28. Arroyo IJ, Hu R, Merino G, Tang BZ, and Peña-Cabrera E (2009). The smallest and one of the brightest. Efficient preparation and optical description of the parent borondipyrromethene system. J. Org. Chem 74, 5719–5722. 10.1021/jo901014w. [PubMed: 19572588]
29. Loudet A, and Burgess K (2007). BODIPY dyes and their derivatives: syntheses and spectroscopic properties. Chem. Rev 107, 4891–4932. 10.1021/cr078381n. [PubMed: 17924696]
30. Lu P, Chung K-Y, Stafford A, Kiker M, Kafle K, and Page ZA (2021). Boron dipyrromethene (BODIPY) in polymer chemistry. Polym. Chem 12, 327–348. 10.1039/D0PY01513J.
31. Peterson JA, Wijesooriya C, Gehrmann EJ, Mahoney KM, Goswami PP, Albright TR, Syed A, Dutton AS, Smith EA, and Winter AH (2018). Family of BODIPY photocages cleaved by single photons of visible/near-infrared light. J. Am. Chem. Soc 140, 7343–7346. 10.1021/jacs.8b04040. [PubMed: 29775298]
32. Goswami PP, Syed A, Beck CL, Albright TR, Mahoney KM, Unash R, Smith EA, and Winter AH (2015). BODIPY-derived photoremovable protecting groups unmasked with green light. J. Am. Chem. Soc 137, 3783–3786. 10.1021/jacs.5b01297. [PubMed: 25751156]
33. Peterson JA, Fischer LJ, Gehrmann EJ, Shrestha P, Yuan D, Wijesooriya C, Smith EA, and Winter AH (2020). Direct photorelease of alcohols from boron-alkylated BODIPY photocages. J. Org. Chem 85, 5712–5717. 10.1021/acs.joc.0c00044. [PubMed: 32216269]
34. Shrestha P, Dissanayake KC, Gehrmann EJ, Wijesooriya CS, Mukhopadhyay A, Smith EA, and Winter AH (2020). Efficient far-red/near-IR absorbing BODIPY photocages by blocking unproductive conical intersections. J. Am. Chem. Soc 142, 15505–15512. 10.1021/jacs.0c07139. [PubMed: 32786742]
35. Slanina T, Shrestha P, Palao E, Kand D, Peterson JA, Dutton AS, Rubinstein N, Weinstain R, Winter AH, and Klán P (2017). In search of the perfect photocage: structure-reactivity relationships in meso-methyl BODIPY photoremovable protecting groups. J. Am. Chem. Soc 139, 15168–15175. 10.1021/jacs.7b08532. [PubMed: 29039200]
36. Koziar JC, and Cowan D (1978). Photochemical Heavy-Atom Effects. Acc. Chem. Res 11, 334–341.
37. Spicer CD (2020). Hydrogel scaffolds for tissue engineering: the importance of polymer choice. Polym. Chem 11, 184–219. 10.1039/c9py01021a.
38. Kölmel DK, and Kool ET (2017). Oximes and hydrazones in bioconjugation: mechanism and catalysis. Chem. Rev 117, 10358–10376. 10.1021/acs.chemrev.7b00090. [PubMed: 28640998]
39. Fairbanks BD, Macdougall LJ, Mavila S, Sinha J, Kirkpatrick BE, Anseth KS, and Bowman CN (2021). Photoclick chemistry: a bright idea. Chem. Rev 121, 6915–6990. 10.1021/acs.chemrev.0c01212. [PubMed: 33835796]
40. Devaraj NK, and Weissleder R (2011). Biomedical applications of tetrazine cycloadditions. Acc. Chem. Res 44, 816–827. [PubMed: 21627112]
41. Pauloehrl T, Delaittre G, Bruns M, Meißler M, Börner HG, Bastmeyer M, and Barner-Kowollik C (2012). Bio)molecular surface patterning by phototriggered oxime ligation. Angew. Chem. Int. Ed 51, 9181–9184. 10.1002/anie.201202684.
42. Zhao J, Lu M, Lai H, Lu H, Lalevée J, Barner-Kowollik C, Stenzel MH, and Xiao P (2018). Delivery of amonafide from fructose-coated nanodiamonds by oxime ligation for the treatment of human breast cancer. Biomacromolecules 19, 451–489. 10.1021/acs.biomac.7b01592.
43. Zhang Z, He C, and Chen X (2018). Hydrogels based on pH-responsive reversible carbon-nitrogen double-bond linkages for biomedical applications. Mater. Chem. Front 2, 1765–1778. 10.1039/c8qm00317c.
44. Sardon H, Zivic N, Kuroishi PK, Dumur F, Gigmes D, and Dove AP (2018). Recent advances and challenges in the design of organic photoacid and photobase generators for polymerizations. Angew. Chem. Int. Ed 58, 10410–10422. 10.1002/anie.201810118.

45. Zhang Z, He C, Rong Y, Ren H, Wang T, Zou Z, and Chen X (2021). A fast and versatile cross-linking strategy via o-phthalaldehyde condensation for mechanically strengthened and functional hydrogels. Natl. Sci. Rev 8, nwaa128. 10.1093/nsr/nwaa128.
46. Zhang X, Xi W, Gao G, Wang X, Stansbury JW, and Bowman CN (2018). O-Nitrobenzyl-Based photobase generators: efficient photoinitiators for visible-light induced thiol-Michael addition photopolymerization. ACS Macro Lett. 7, 852–857. 10.1021/acsmacrolett.8b00435. [PubMed: 35650759]
47. Taylor MT, Blackman ML, Dmitrenko O, and Fox JM (2011). Design and synthesis of highly reactive dienophiles for the tetrazine-trans-cyclooctene ligation. J. Am. Chem. Soc 133, 9646–9649. 10.1021/ja201844c. [PubMed: 21599005]
48. Blackman ML, Royzen M, and Fox JM (2008). Tetrazine ligation: fast bioconjugation based on inverse-electron-demand Diels-Alder reactivity. J. Am. Chem. Soc 130, 13518–13519. 10.1021/ja8053805. [PubMed: 18798613]
49. Schmidt P, Zhou L, Tishinov K, Zimmermann K, and Gillingham D (2014). Dialdehydes lead to exceptionally fast bioconjugations at neutral pH by virtue of a cyclic intermediate. Angew. Chem. Int. Ed 53, 10928–10931. 10.1002/anie.201406132.
50. Truong VX, and Barner-Kowollik C (2021). Red-light driven photocatalytic oxime ligation for bioorthogonal hydrogel design. ACS Macro Lett. 10, 78–83. 10.1021/acsmacrolett.0c00767. [PubMed: 35548995]
51. Sitkowska K, Feringa BL, and Szymański W (2018). Green-light-Sensitive BODIPY photoprotecting groups for amines. J. Org. Chem 83, 1819–1827. 10.1021/acs.joc.7b02729. [PubMed: 29369628]
52. Hall HK (1964). Correlation of the base strengths of amines. J. Am. Chem. Soc 86, 5709. 10.1021/ja01078a602.
53. Benzylhydrazine | 555-96-4.
54. O-Benzylhydroxylamine | 622-33-3.
55. Jia F, Song J, Kubiak JM, Onoda M, Santos PJ, Sano K, Holten-Andersen N, Zhang K, and MacFarlane RJ (2021). Brush polymers as nanoscale building blocks for hydrogel synthesis. Chem. Mater 33, 5748–5756. 10.1021/acs.chemmater.1c01585.
56. Rong Y, Zhang Z, He C, and Chen X (2020). Bioactive polypeptide hydrogels modified with RGD and N-cadherin mimetic peptide promote chondrogenic differentiation of bone marrow mesenchymal stem cells. Sci. China Chem 63, 1100–1111. 10.1007/s11426-020-9772-0.
57. Jonker AM, Bode SA, Kusters AH, van Hest JCM, and Löwik DWPM (2015). Soft PEG-hydrogels with independently tunable stiffness and RGDS-content for cell adhesion studies. Macromol. Biosci 15, 1338–1347. 10.1002/mabi.201500110. [PubMed: 26097013]
58. Bellis SL (2011). Advantages of RGD peptides for directing cell association with biomaterials. Biomaterials 32, 4205–4210. 10.1016/j.biomaterials.2011.02.029. [PubMed: 21515168]

Highlights

- Efficient photouncaging and ligation using optimized BODIPY scaffolds
- Rapid and mild hydrogel synthesis in 90 wt % water using green light
- Precise spatial control for high-resolution hydrogel patterning
- Precise temporal control for tunable hydrogel moduli

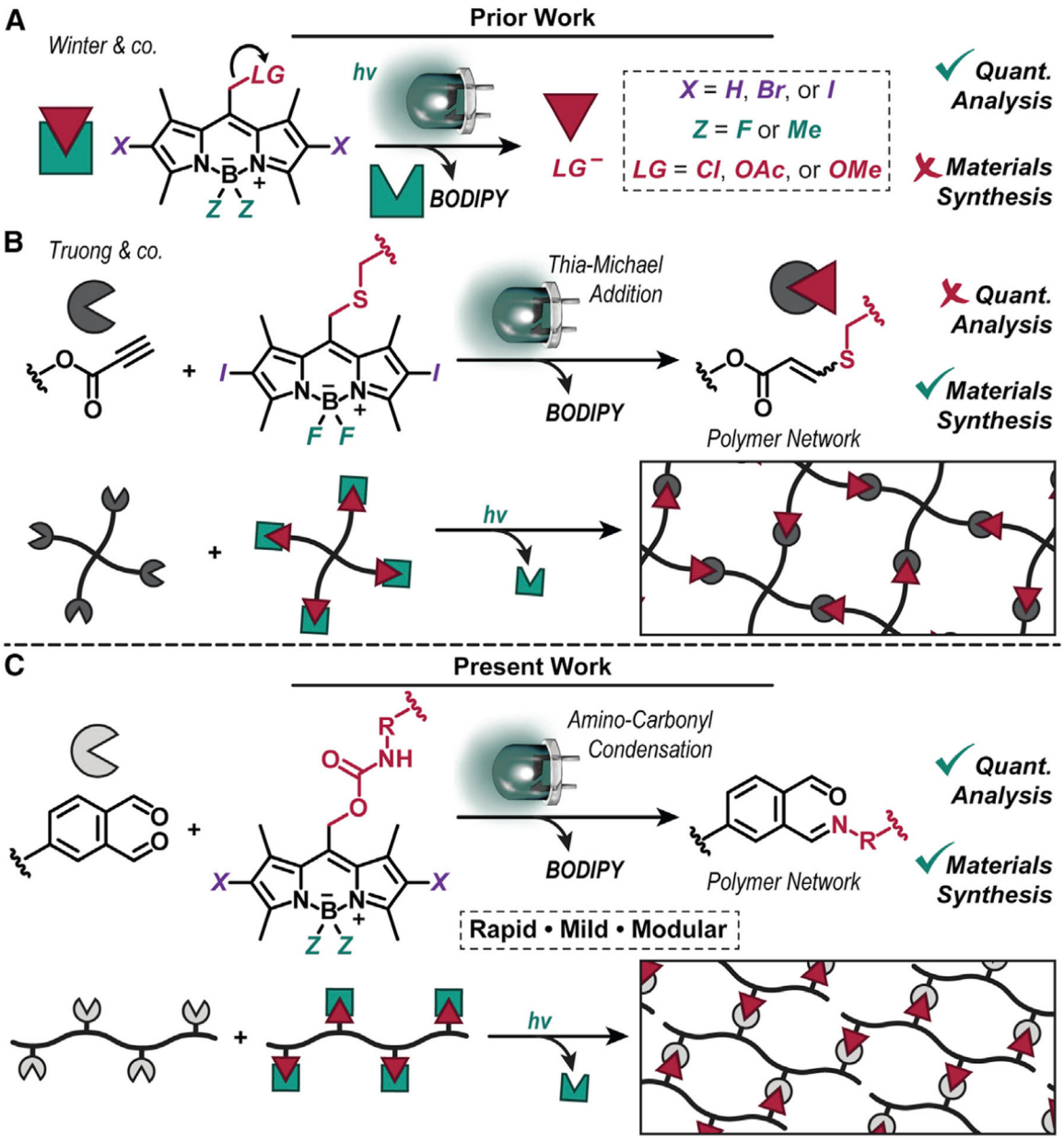

Figure 1. Overview of prior and present BODIPY photocage efforts

(A) Prior work by Winter and coworkers to quantify the photouncaging yields of chloride, acetate, and methoxy leaving groups as a function of BODIPY structure.

(B) Prior work by Truong and coworkers to prepare hydrogels via photoactivated thia-Michael addition.

(C) Present work quantifying the photouncaging yields of amine, hydrazine, and aminooxy leaving groups as a function of BODIPY structure and its utility in the preparation of hydrogels via rapid and mild amino-carbonyl condensation.

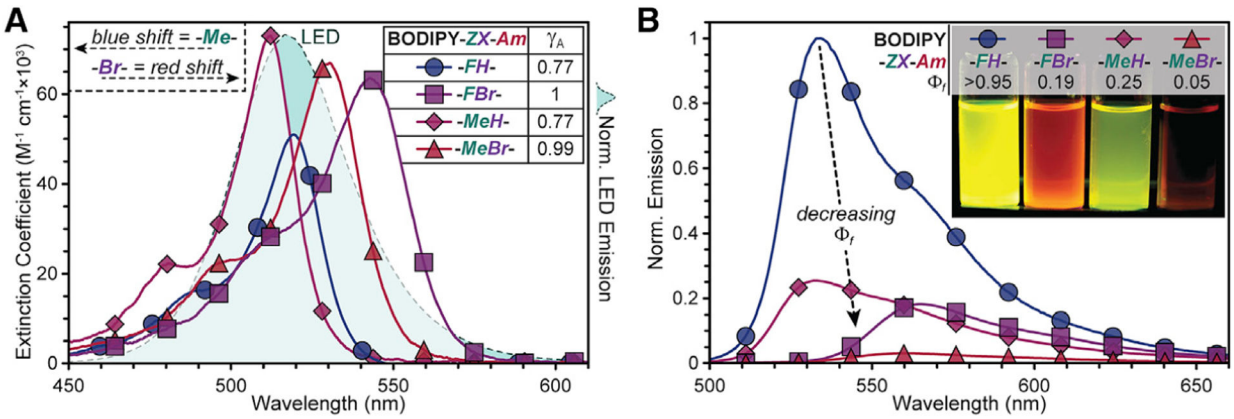

Figure 2. Steady-state photophysical characterization of BODIPY-ZX-Am derivatives

(A) Absorption spectra of BODIPY-ZX-Am in acetonitrile (concentration [conc.] ~10^{-6} M) overlaying a normalized green LED emission profile. Table inset provides normalized values of photons absorbed γ_A. Data points collected every 1 nm, with symbols indexed for clarity. (B) Emission spectra of BODIPY-ZX-Am in acetonitrile (conc. ~10^{-6} M) to determine fluorescence quantum yield Φ_F values, given in the table inset. R6G was used as the fluorescence standard. Data points collected every 1 nm, with symbols indexed for clarity. Inset shows images of solutions irradiated by 365 nm handheld UV lamp.

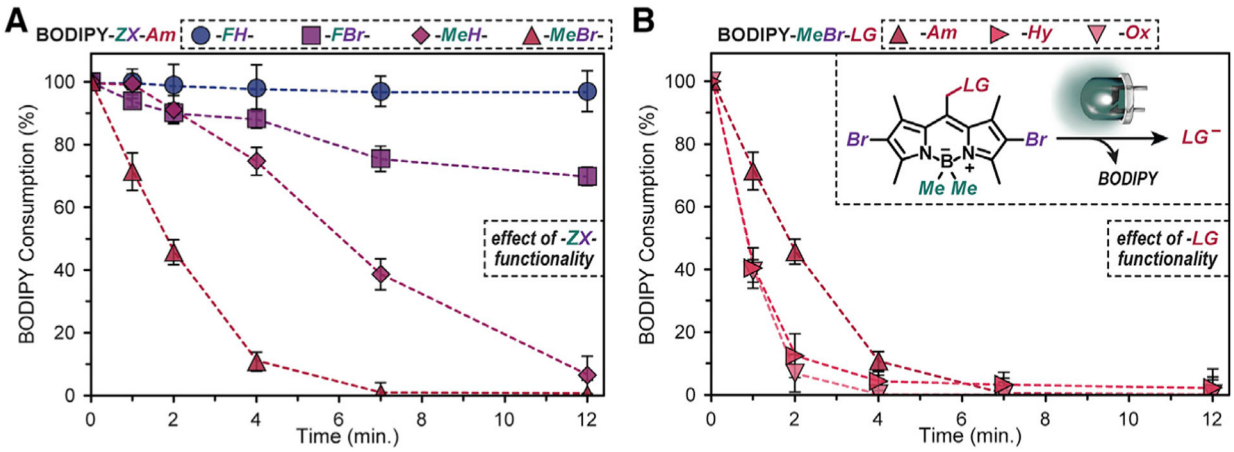

Figure 3. Degradation of BODIPY photocages (0.53 mM in 4:1 CH_3CN:H_2O) with green light (λ_{max} = 520 nm, 10 mW/cm^2)

(A) Influence of -ZX- functionality on BODIPY-Am photocage degradation over time. Dashed lines connect data points as a guide for the eye. Error bars represent ±1 SD from the mean.

(B) Influence of -LG functionality on BODIPY-MeBr photocage degradation over time. Dashed lines connect data points as a guide for the eye. Error bars represent ±1 SD from the mean.

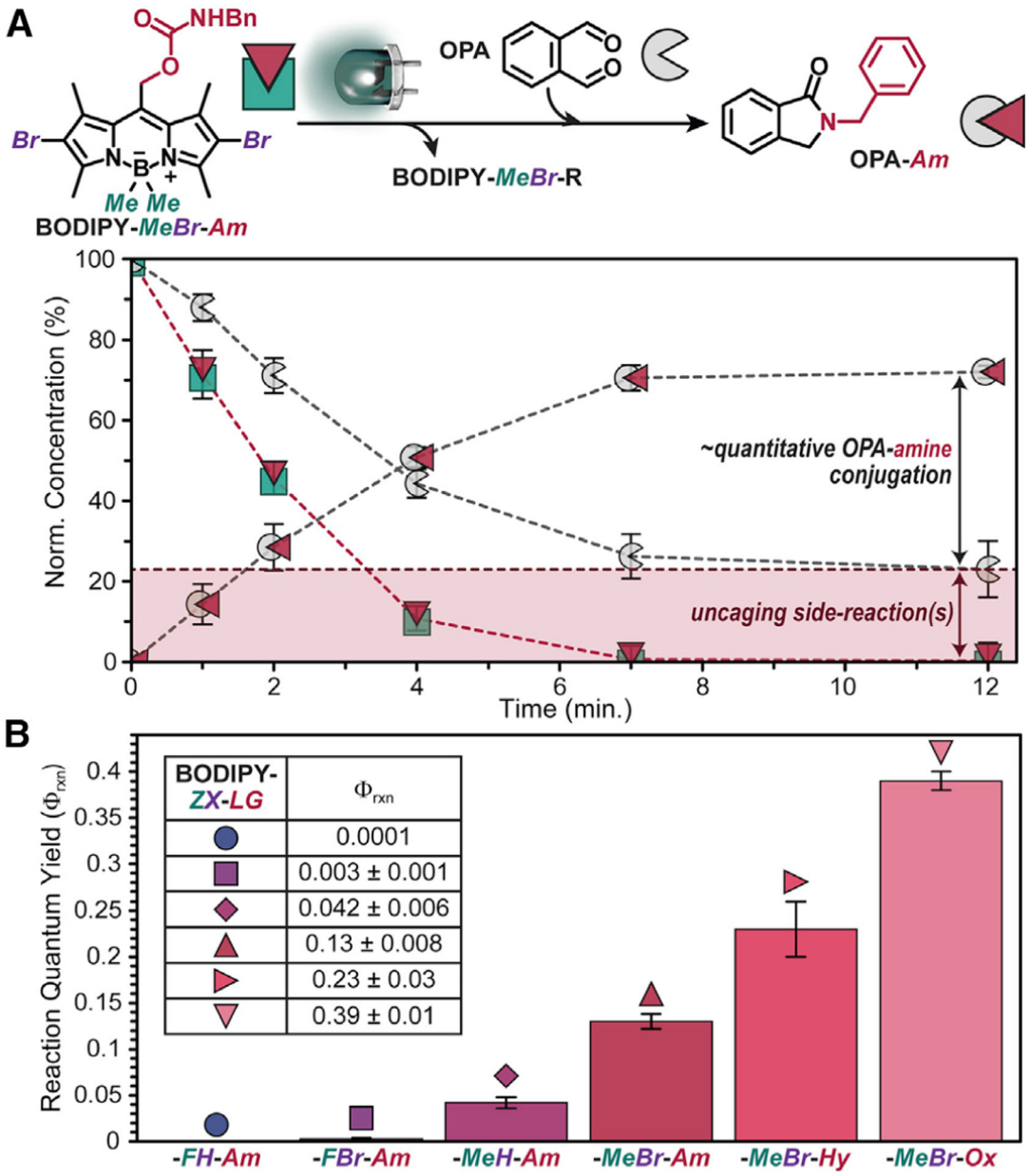

Figure 4. Photouncaging kinetics and quantum yields

(A) Schematic of OPA-conjugation reaction and representative kinetics for BODIPY-MeBr-Am, OPA, and OPA-Am during irradiation. Dashed lines connect data points as a guide for the eye. Error bars represent ±1 SD from the mean.

(B) Reaction quantum yields for OPA conjugation induced by irradiating different BODIPY-ZX-LG photocages in the presence of OPA. Absolute values provided in the table inset. Error bars represent ±1 SD from the mean.

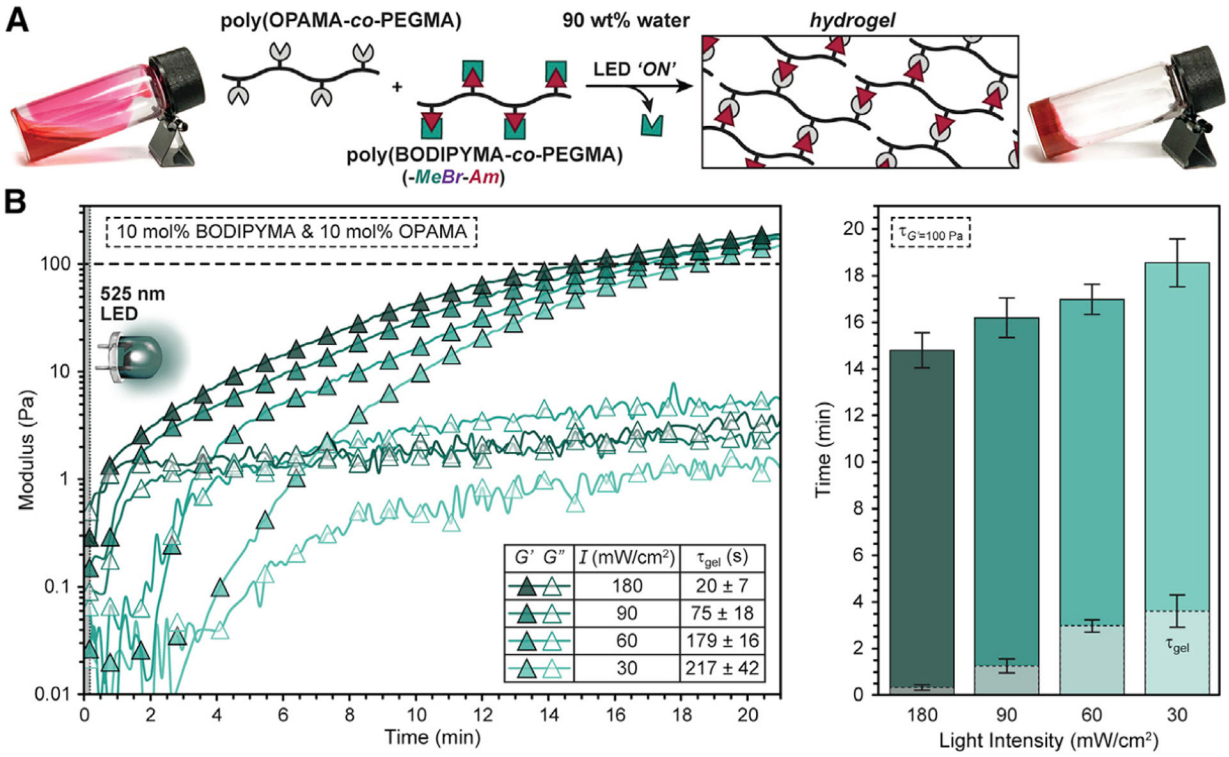

Figure 5. Gelation and viscoelastic properties

(A) Schematic of hydrogel fabrication via photoinduced crosslinking with representative images of vial inversion test for pre- (left) and post- (right) irradiation.

(B) Photorheology of poly(OPAMA-*co*-PEGMA) (5 wt %) and poly(BrBODIPYMA-co-PEGMA) (5 wt %) mixtures in H_2O under ambient conditions. Irradiation with a 525 nm LED at the listed intensities occurred after a 15 s dark period (gray bar). The time to gelation τ_{gel} is provided in the table inset and bar graph (right), along with the time to a self-supporting gel defined as G′ = 100 Pa ($\tau_{G'}$ =100 Pa). Rheology data points collected every 10 s, with symbols indexed for clarity. G', storage modulus; G'', loss modulus.

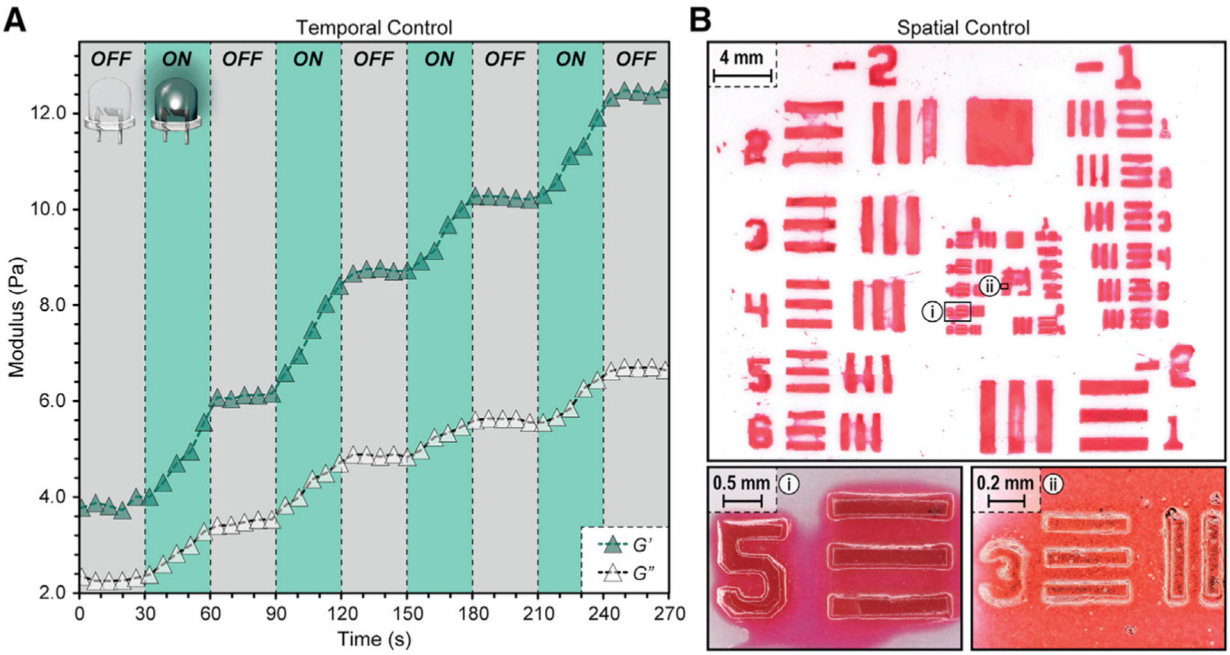

Figure 6. Spatiotemporal control

(A) Photorheological characterization of poly(OPAMA-*co*-PEGMA) (5 wt %) and poly(BrBODIPYMA-co-PEGMA) (5 wt %) mixtures in H_2O under ambient conditions during LED on/off cycling to demonstrate temporal control. Data points collected every ~10 s, with symbols indexed for clarity. G', storage modulus; G'', loss modulus.

(B) Digital microscopy images of photopatterned hydrogels at different magnifications to demonstrate spatial control. A negative 1951 USAF resolution photomask was used for patterning of poly(OPAMA-*co*-PEGMA) (5 wt %) and poly(BrBODIPYMA-*co*-PEGMA) (5 wt %) mixtures in H_2O under ambient conditions. A resolution limit of 5 lp/mm (= 100 μm line width) was obtained under these conditions: 250 μm thick, 30 mW/cm^2 525 nm LED, 45 min irradiation.

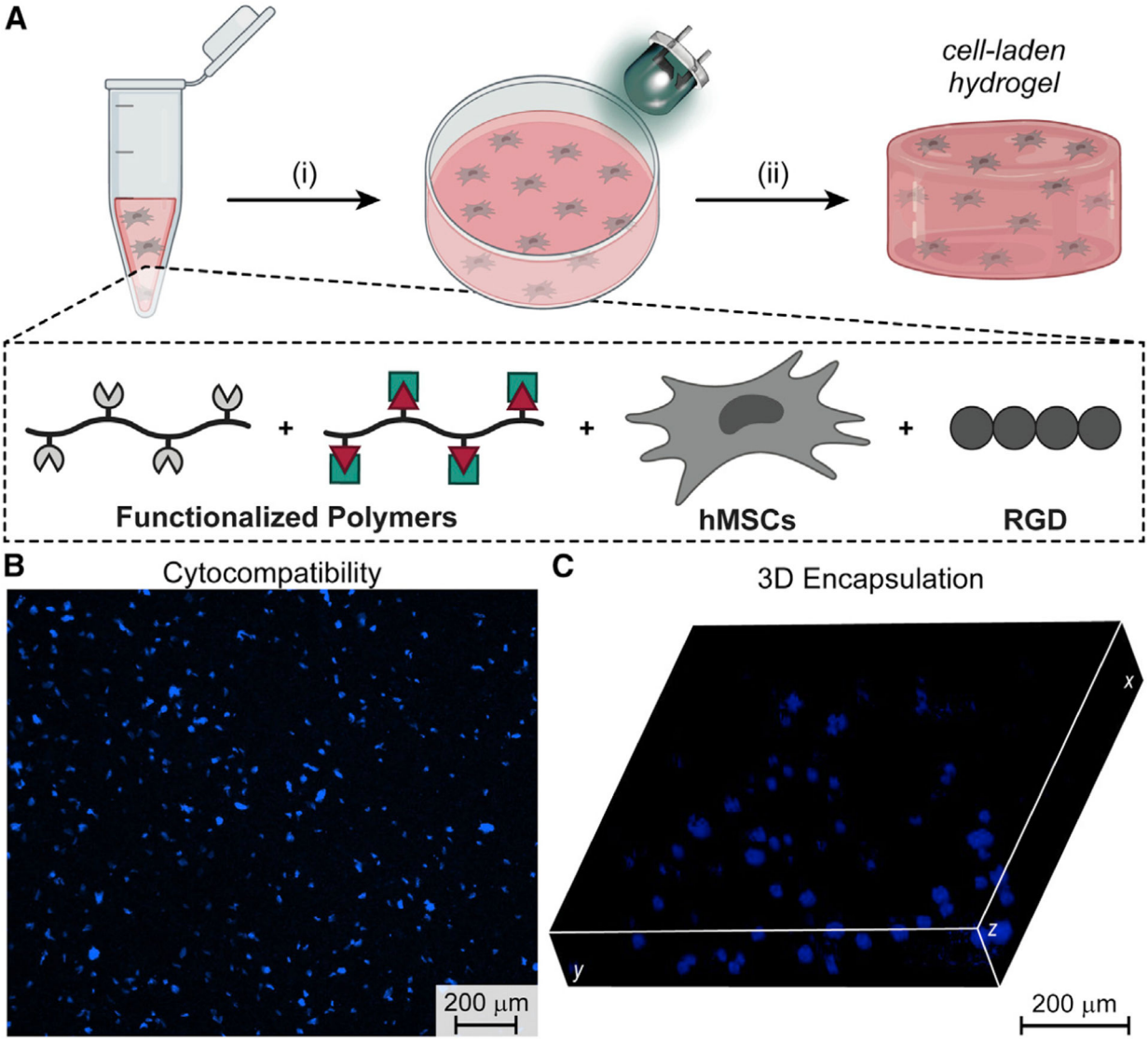

Figure 7. Cell studies

(A) Schematic of the protocol used for cellular encapsulation. A precursor solution was prepared with poly(OPAMA-*co*-PEGMA) (5 wt %), poly(BrBODIPYMA-*co*-PEGMA) (5 wt %), RGD (2 mM), and hMSCs (1×10^6 cells/mL), added to a glass-bottom mini Petri dish, and crosslinked for 5 min with a 525 nm LED.

(B) Cell viability 30 min post-encapsulation is shown in this fluorescent microscope image of calcein blue AM-stained cells.

(C) A volume reconstruction containing cells stained with Cell Tracker 30 min post-encapsulation illustrating cellular distribution through multiple planes of the hydrogel.

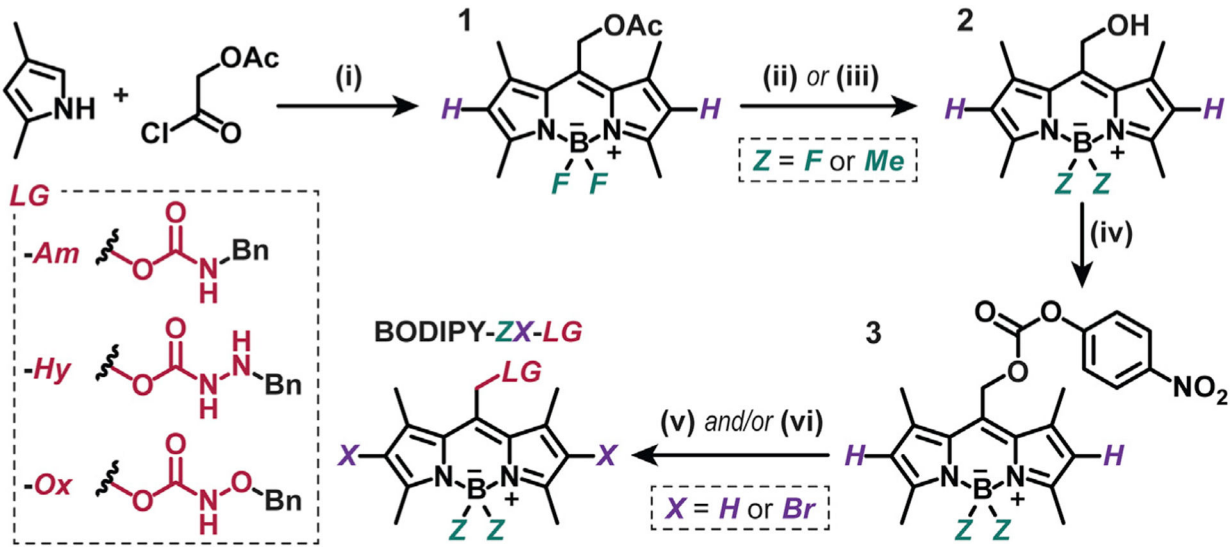

Scheme 1. Synthesis of BODIPY-ZX-LG photocages

Conditions: (i) diisopropylethylamine, boron trifluoride etherate; (ii) 1 M NaOH(aq); (iii) methylmagnesium bromide; (iv) 4-nitrophenyl chloroformate, diisopropylethylamine, pyridine; (v) benzylamine, pyridine; (vi) *N*-bromosuccinimide. -Am, benzylamine, pyridine; -Hy, benzyl hydrazine, 4-dimethylaminopyridine; -Ox, benzyl hydroxylamine, 4-dimethylaminopyridine.

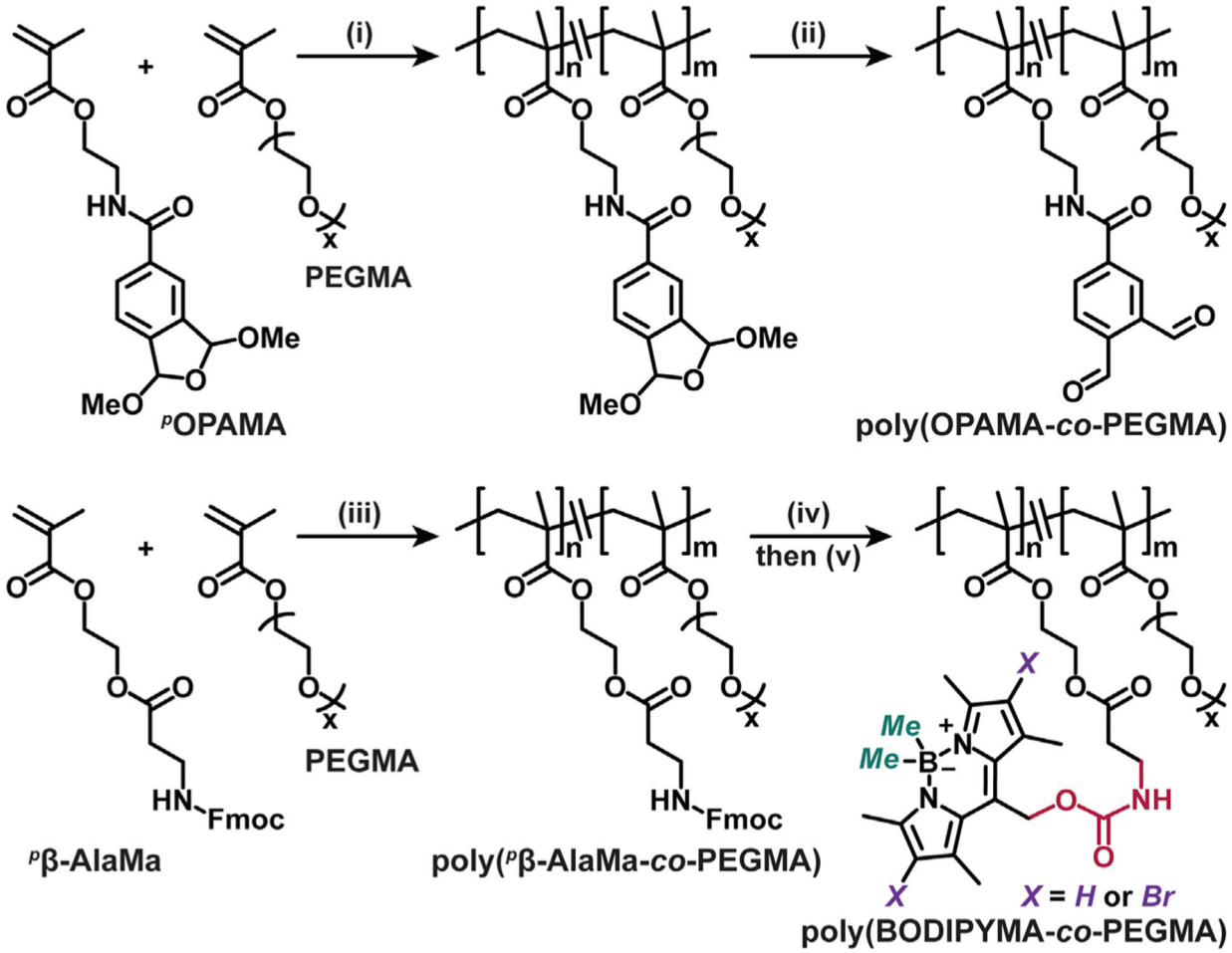

Scheme 2. Syntheses of poly(OPAMA-co-PEGMA) (top) and poly(BODIPYMA-*co*-PEGMA) (bottom)

(i) Phenylbis(2,4,6-trimethylbenzoyl)phosphine oxide (BAPO), 365 nm LED (30 mW/cm^2), 1 h; (ii) trifluoroacetic acid (20 wt % in H_2O), 1 h; (iii) azobisisobutyronitrile (AIBN), 70°C, 12 h; (iv) piperidine (20 wt % in DMF), 15 min; and (v) BODIPY compound 3 (X = H or Br), pyridine, 12 h.